Article

Current Biology

Auxin-dependent control of cytoskeleton and cell shape regulates division orientation in the *Arabidopsis* embryo

Graphical abstract

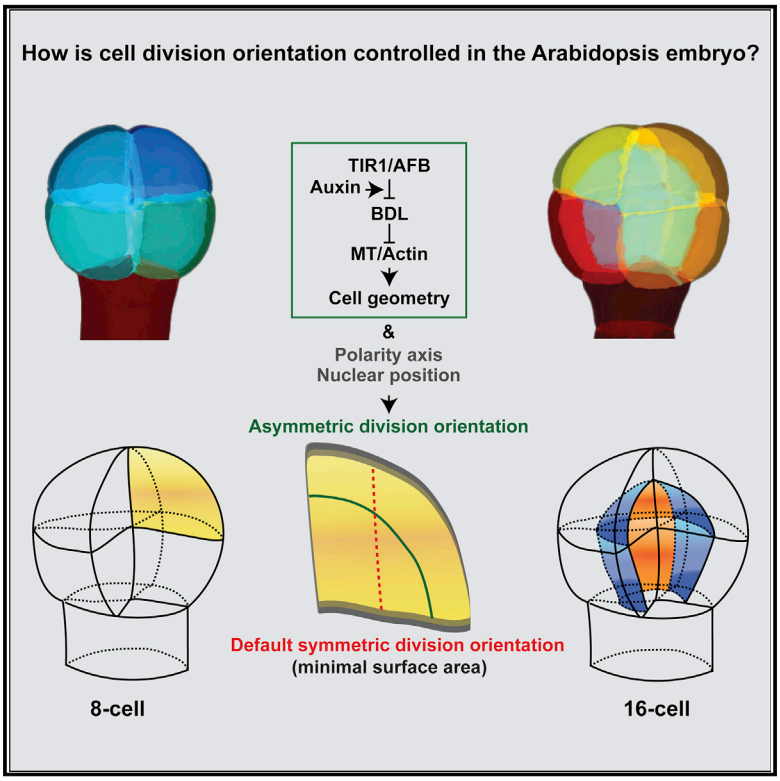

Authors

Prasad Vaddepalli, Thijs de Zeeuw, Sören Strauss, ..., João Jacob Ramalho, Richard S. Smith, Dolf Weijers

Correspondence

prasad.vaddepalli@zmbp.uni-tuebingen.de (P.V.), dolf.weijers@wur.nl (D.W.)

In brief

By combining 3D imaging of cell shapes, nuclear and polarity markers, transcriptome profiling, genetic analysis, and targeted perturbation of cytoskeletal structures, Vaddepalli, de Zeeuw et al. reveal that auxin-dependent control of cell division orientation in *Arabidopsis* embryos involves regulation of cytoskeleton and cell shape.

Highlights

- Auxin responses regulate directional cell expansion in *Arabidopsis* embryos
- Cell shape and division orientation are tightly coupled
- Transcriptome analysis identifies MT-associated IQD proteins in division control
- Cytoskeletal dynamics control division orientation

Vaddepalli et al., 2021, Current Biology *31*, 4946–4955
November 22, 2021
https://doi.org/10.1016/j.cub.2021.09.019

CellPress

CellPress
OPEN ACCESS

Current Biology

Article

Auxin-dependent control of cytoskeleton and cell shape regulates division orientation in the *Arabidopsis* embryo

Prasad Vaddepalli,[1,5,7,8,*] Thijs de Zeeuw,[1,6,7] Sören Strauss,[2] Katharina Bürstenbinder,[3] Che-Yang Liao,[1] João Jacob Ramalho,[1] Richard S. Smith,[2,4] and Dolf Weijers[1,9,10,*]

[1]Laboratory of Biochemistry, Wageningen University, Stippeneng 4, 6708 Wageningen, the Netherlands
[2]Department of Comparative Development and Genetics, Max Planck Institute for Plant Breeding Research, Carl-von-Linne-Weg 10, Cologne, Germany
[3]Department of Molecular Signal Processing, Leibniz Institute of Plant Biochemistry, Weinberg 3, Halle (Saale), Germany
[4]John Innes Centre, Norwich Research Park, Norwich NR4 7UH, UK
[5]Present address: Center for Plant Molecular Biology (ZMBP), University of Tübingen, Auf der Morgenstelle 32, 72076 Tübingen, Germany
[6]Present address: Laboratory of Plant Physiology, Wageningen University, Droevendaalsesteeg 1, Wageningen, the Netherlands
[7]These authors contributed equally
[8]Twitter: @me_prasad
[9]Twitter: @dolfweijers
[10]Lead contact
*Correspondence: prasad.vaddepalli@zmbp.uni-tuebingen.de (P.V.), dolf.weijers@wur.nl (D.W.)
https://doi.org/10.1016/j.cub.2021.09.019

SUMMARY

Premitotic control of cell division orientation is critical for plant development, as cell walls prevent extensive cell remodeling or migration. While many divisions are proliferative and add cells to existing tissues, some divisions are formative and generate new tissue layers or growth axes. Such formative divisions are often asymmetric in nature, producing daughters with different fates. We have previously shown that, in the *Arabidopsis thaliana* embryo, developmental asymmetry is correlated with geometric asymmetry, creating daughter cells of unequal volume. Such divisions are generated by division planes that deviate from a default "minimal surface area" rule. Inhibition of auxin response leads to reversal to this default, yet the mechanisms underlying division plane choice in the embryo have been unclear. Here, we show that auxin-dependent division plane control involves alterations in cell geometry, but not in cell polarity axis or nuclear position. Through transcriptome profiling, we find that auxin regulates genes controlling cell wall and cytoskeleton properties. We confirm the involvement of microtubule (MT)-binding proteins in embryo division control. Organization of both MT and actin cytoskeleton depends on auxin response, and genetically controlled MT or actin depolymerization in embryos leads to disruption of asymmetric divisions, including reversion to the default. Our work shows how auxin-dependent control of MT and actin cytoskeleton properties interacts with cell geometry to generate asymmetric divisions during the earliest steps in plant development.

INTRODUCTION

Mechanisms controlling plant division plane orientation have been an area of focus for over a century.[1–3] Starting from the establishment of the early embryo to the development of post-embryonic tissues and organs, plants need to constantly calibrate the coordination between cellular and genetic inputs for proper cell and tissue patterning. Failure in the coordination leads to aberrant phenotypes with severe developmental defects.[4–6] Proliferative mitotic cell divisions select symmetric division plane, resulting in cells with approximately equal size. In formative divisions, however, division planes strongly deviate from the symmetric position, leading to daughter cells of different sizes. Such asymmetric divisions often lead to the formation of new cell identities and tissue layers, and these divisions can thus lead to differential developmental fates.

Plant cells by default divide along the minimal surface area (in 3D) following the "shortest wall" (in 2D) rule.[7] Thus, cell geometry influences its plane of division and therefore is a fundamental input in determining the size and shape of daughter cells. Genetic regulation can interfere with the default symmetric division to facilitate division plane orientation.[8] Recent evidence suggests that cytoskeleton dynamics may bridge the coordination of geometric and genetic input to influence the re-orientation of the division plane.[9,10] During the first asymmetric division of the zygote and in lateral root founder cells, dynamics of cytoskeletal pattern determine the correct orientation of division plane. In both these systems, however, cells are elongated, and the various orientations of division are dramatically different in terms of surface area and volume partitioning. A key question is whether similar mechanisms operate in smaller, polyhedral cells, where such differences are less extreme. The signaling cue for

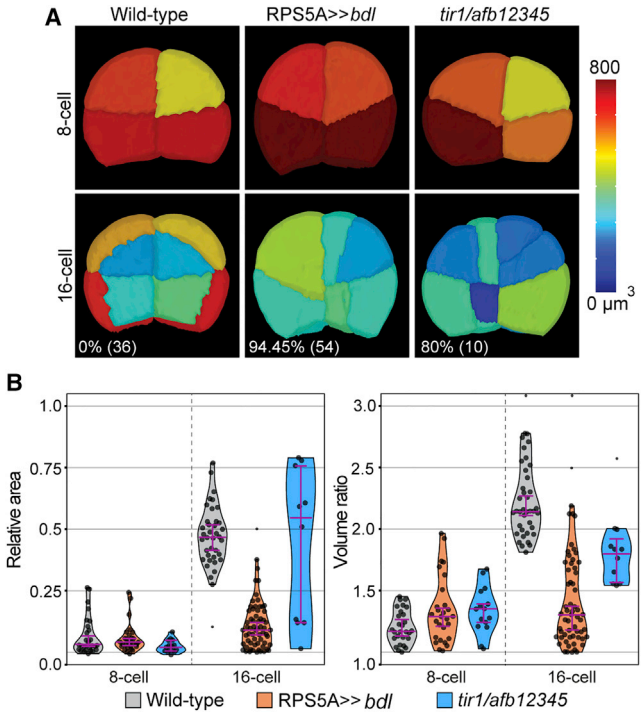

Figure 1. Auxin response is required for asymmetric embryonic cell division

(A) 3D comparison of wild-type, *RPS5A>>bdl*, and *tir1/afb* mutant embryos. Cell colors correspond to cellular volume as indicated in the color scale. The percentage of symmetric orientation defects at 16-cell stage and number of cell pairs analyzed (% (n)) are indicated at the bottom.

(B) Violin plots representing distribution of division plane areas and volume ratios. The relative area is the actual division plane normalized by the smallest (0) and largest (1) possible division wall areas. Division planes were simulated through the center point of the actual division plane between two sister cells. The cell volume ratio plot of the daughter cells resulting from these divisions is presented in the right panel.

Whiskers represent median ± 95% confidence intervals (CIs). At least two individual embryos were used per condition.

biasing division plane orientation likely involves cell polarity mechanisms,[11] but how the intracellular position of polarity proteins direct division plane orientations remains elusive. In several cell types, nuclear position co-aligns with the preprophase band (PPB),[12] and migration of the nucleus is correlated with positioning of the division plane wall in the zygote, lateral root founder cells, and leaf epidermis.[9,10,13] Again, all those cell types are either large, relative to nuclear size, or have extreme aspect ratios, and it remains a question whether the same principles apply to division control in other types of cells.

Developing from a fertilized egg cell, the early plant embryo is a hotspot for formative events: new cell types are established with many divisions, which in *Arabidopsis* are highly predictable.[14,15] Using advanced imaging and cellular segmentation approaches, a 3D description of early *Arabidopsis* embryogenesis has been generated.[8] From this work, it surfaced that divisions leading to the 2-, 4-, and 8-cell embryo stages follow the minimal surface area rule, corroborating classical (2D) models from the 19th century. However, the next asymmetric divisions that generate the protoderm and inner cells at the 16-cell stage deviated from this rule. Using mutant embryos in which response to the plant hormone auxin was blocked by ubiquitous expression of a transcriptional repressor (*RPS5A>>bdl*),[16] it was demonstrated that transcriptional response to auxin is required to suppress the geometric default division, implicating that the regulation of oriented cell division by geometric and genetic cues can be uncoupled. Thus, the 8-cell *Arabidopsis* embryo represents a unique case where the activity of a transcriptional regulator (bdl) allows to switch between default, symmetric, and regulated asymmetric division. Based on a more recent computational model, it has been proposed that all division planes observed in wild-type and mutant cells conform to a default rule, provided that new walls can be curved when inserted.[17] In the same study, it was suggested that, also in these cells, nuclear position may provide input into division plane position.[17] Analysis of live embryos found little to no curvature in newly formed walls,[8] and it is therefore an open question through what cellular processes, genes, and mechanisms the division orientation in early embryos is controlled. Conceptually, the axis of cell polarity, cell shape, and nuclear position can each influence and collectively interact to guide division plane position and orientation. The auxin-dependent switch in ultimate division plane allows to dissect at what point these processes can be regulated. Here, we explore mechanisms underlying division plane selection in the embryo.

RESULTS

TIR1/AFB-dependent auxin response controls cell division orientation in the early embryo

Auxin promotes degradation of AUX/IAA proteins through TIR1/AFB receptors, thus promoting ARF-dependent gene expression.[18] A mutation in the degron of Aux/IAA proteins prevents interaction with TIR1/AFB proteins, causing accumulation of mutant protein and permanent ARF inhibition.[16,19] Expression of mutant iaa12/bdl protein in early embryos (*RPS5A>>bdl*) prevents asymmetric divisions at the 8-cell stage.[8] However, because the mutant protein can accumulate to unnaturally high levels, this may lead to inhibition effects beyond the normal activity of auxin. Hence, it is not yet clear whether an endogenous auxin response process controls division orientation.

Therefore, we scrutinized 3D division orientation in mutant embryos lacking all 6 TIR1/AFB receptors, the *tir1/afb* sextuple (*tir1afb12345*) mutant.[20] This mutant arrests during embryogenesis with defects that superficially resemble those observed in *RPS5A>>bdl* embryos.[20] To compare division defects more directly, we made use of a sextuple homozygote that carries a heterozygous complementation transgene carrying TIR1-mOrange2::AFB5-mCherry::AFB2-mCitrine.[20] The hemizygous *tir1afb12345* mutant thus has 25% sextuple mutant progeny.[20] Cell segmentation analysis using MorphoGraphX[8,21] on mutant embryos confirmed the resemblance of division plane defects with the *RPS5A>>bdl* phenotype (Figure 1A). Division plane orientation did, however, show variability. Next, we measured volumes of pairs of sister cells at 8- and 16-cell stages to determine the volume distribution ratios as a proxy for division (a-) symmetry. We also analyzed the division plane surface area relative to the minimal and maximal planes cutting through the center of the actual division.[8] In *tir1afb12345* mutant embryos, divisions leading to 8-cell embryos are symmetric and use the

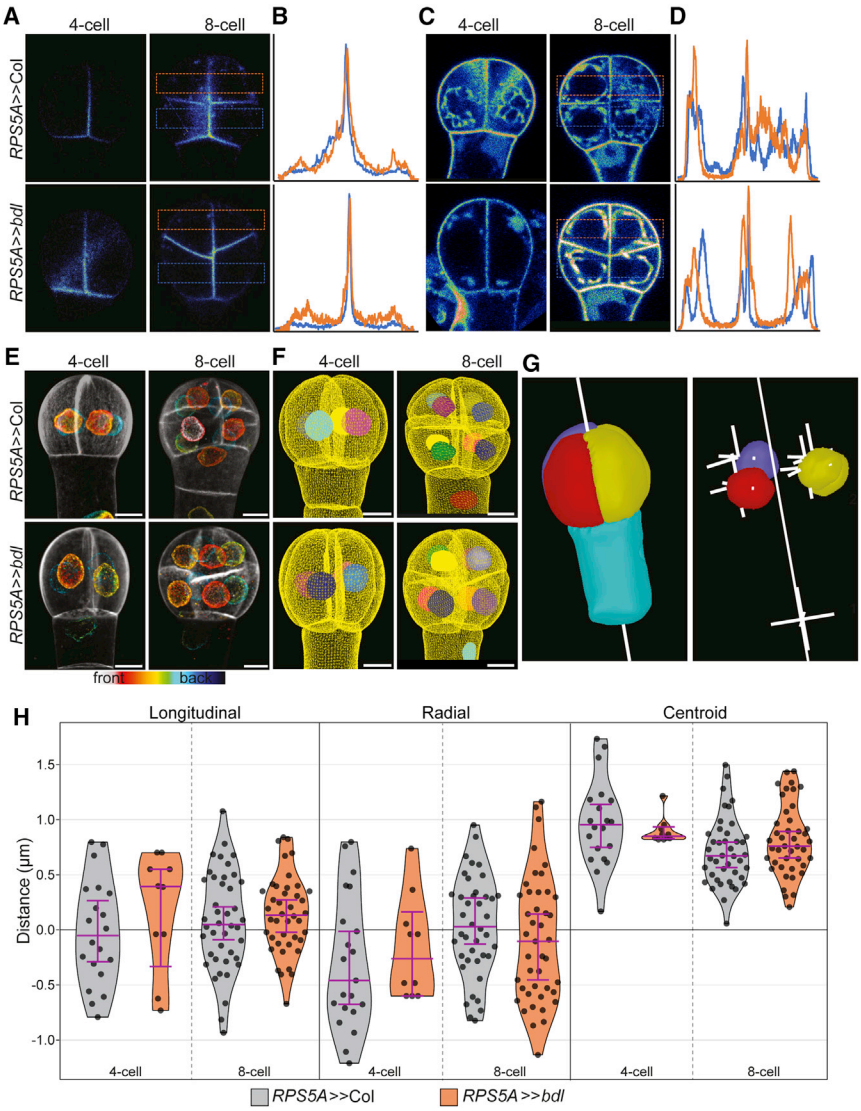

Figure 2. Analysis of polarity and nuclear position in wild-type and *bdl* embryos

(A and C) Single optical sections of (A) inner membrane marker BOR1-mCitrine (ACE-W03) and (C) outer membrane marker mCherry-NIP5;1 (ACE-W04).

(B and D) Fluorescence intensity profiles of upper (orange) and lower (blue) tier cells generated by the regions of interest (ROIs) shown as dashed boxes in (A) and (C), respectively.

(E–H) Nuclear position analysis.

(E) Maximum intensity projection of depth-coded stacks of nuclear envelopes labeled by AtNUP54-GFP (ACE-W11) reporter line with SCRI Renaissance 2200 (SR2200)-stained cell walls.

(F) Visualization of segmented nuclei within segmented cell meshes. Scale bars, 5 μm.

(G) A central axis is defined through the embryo proper for analysis of nuclear position within the cell. From this axis, longitudinal and radial distances from each cell centroid are defined.

(H) Analysis of nucleus position relative to cellular centroid position within embryos. Average distances are shown for individual cells. The distance to the centroid is absolute and not directed and therefore cannot be below 0.

Whiskers represent median ± 95% CIs. Measurements were done on 9–43 individual cells and corresponding nuclei from at least 4–8 different individual embryos per condition.

minimal surface area, similar to wild-type and *RPS5A>>bdl* embryos (Figure 1B). In *tir1afb12345* mutant embryos, divisions leading to 16-cell embryos show a high variation in relative division plane surface area and volume ratios ranging between the values seen for *RPS5A>>bdl* and those in wild-type (Figure 1B). The average division is therefore more symmetric than wild-type. The observed variation in division represents a spectrum of division plane defects that clearly include those observed in *RPS5A>>bdl* embryos but also display weaker aberrations. It is unclear whether this is due to residual TIR1/AFB activity in the hextuple mutant. Nonetheless, this analysis shows that endogenous auxin response is required for promoting asymmetric cell division in the embryo through regulating division plane orientation.

Cell shape, not polarity axis or nuclear position, correlates with division orientation

To analyze the role of cell polarity, nuclear position, and cell shape in division orientation, we focused on 4-cell and 8-cell stage embryos that give rise to the 8-cell and 16-cell embryos, respectively. Because outer-inner cell polarity is established early in wild-type embryos,[22] and because divisions at the 8-cell stage in wild-type are strictly aligned with this polarity axis, it is conceivable that the division defects in *RPS5A>>bdl* embryos reflect a loss of polarity. We addressed this question by imaging the inner *WOX2$_{pro}$:BOR1-mCitrine* (ACE-W03) and outer *WOX2$_{pro}$:mCherry-NIP5;1* (ACE-W04)[22] domain markers in *RPS5A>>bdl* and wild-type control (*RPS5A>>*Col) embryos. Despite characteristic defects in cell division orientation, no difference in BOR1-mCitrine and mCherry-NIP5;1 localization could be detected between *RPS5A>>*Col and *RPS5A>>bdl* embryos (Figures 2A–2D). As in wild-type embryos, the BOR1 marker is enriched at the inner cell membranes (Figures 2A and 2B) and mCherry-NIP5;1 to the outer membranes (Figures 2C and 2D) of defective 4-cell- and 8-cell-stage *RPS5A>>bdl* embryos. Thus, early outer-inner polarity axis establishment appears independent of transcriptional auxin response and the failure to divide asymmetrically in the mutant is likely not caused by global loss of polarity.

Asymmetric cell division in the zygote, in lateral root founder cells, and in meristemoid mother cells involve nuclear migration to the future division site, implying a strong association of division plane position with nuclear position.[9,10,13,23] Compared to these systems, early embryonic cells have distinct cell geometry, and our previous observations on wild-type embryos suggested

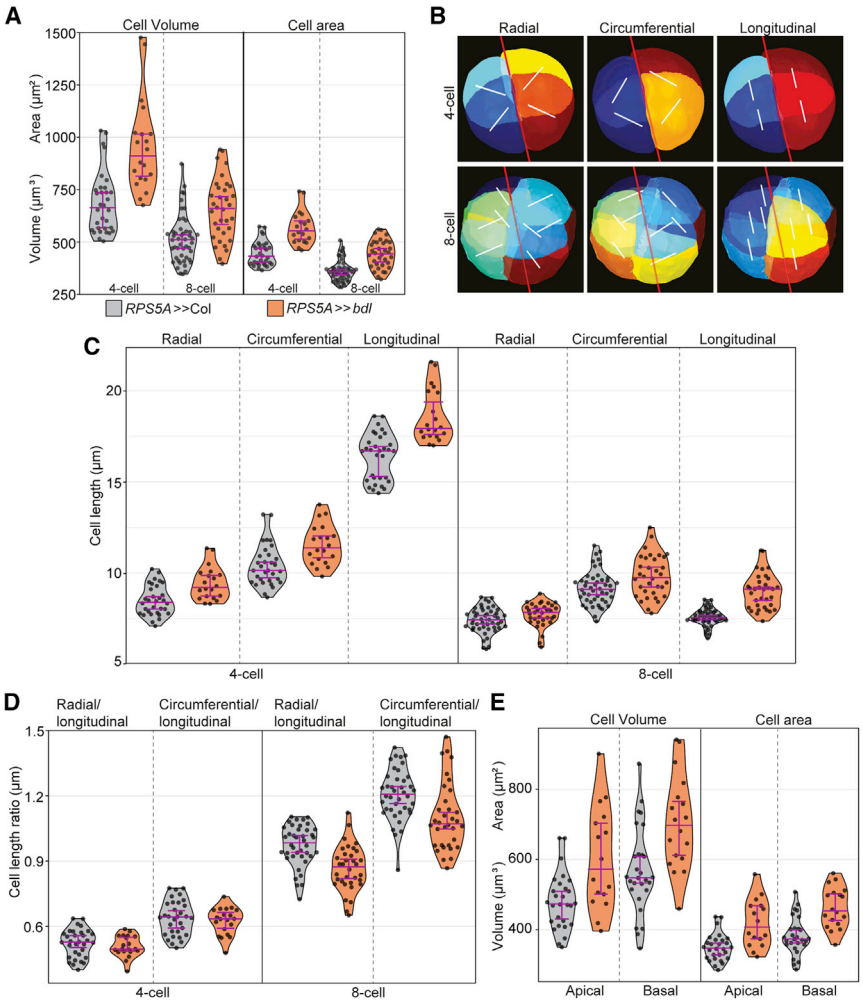

Figure 3. 3D cell shape analysis of wild-type and *bdl* embryos

(A) Average cell volume (in μm^3) and cell surface area (in μm^2) are shown.

(B) Segmented wild-type embryos indicating the axis for measurements shown in (C). First, a central axis (red line) was defined for the pro-embryo. Relative from this axis, circumferential, radial, and longitudinal directions were defined, and the cell length was measured along those directions.

(C) Average radial, circumferential, and longitudinal cell lengths (in μm) are shown.

(D) Their ratios are shown to quantify cell shape changes.

(E) Average cell volume (in μm^3) and cell surface area (in μm^2) in apical and basal cells of 8-cell embryos.

Whiskers represent median ± 95% CIs. Measurements were done on 20–48 individual embryonic cells from at least 5 individual embryos per condition. See also Figure S1.

that the nucleus occupies a relatively large part of the cell, limiting its ability to move.[22] A recent report proposed that nuclear position could constrain both symmetric and asymmetric division plane position in early *Arabidopsis* embryo cells.[17] We explored this hypothesis in *RPS5A>>bdl* mutant embryo cells, which exhibit a consistent switch from asymmetric to symmetric division planes at the 16-cell stage. We also asked whether changes in the position of the nucleus correlate with the switch in division orientation in *RPS5A>>bdl* embryo cells. We introduced the embryonic nuclear envelope marker *$WOX2_{pro}$:NUP54-GFP* (ACE-W11)[22] into the *RPS5A-GAL4* background and crossed this line with wild-type or upstream activating sequence (UAS)-bdl to visualize the nuclear volume in *RPS5A>>bdl* and wild-type control embryos. We did not observe conspicuous differences in nuclear morphology between the two genotypes (Figure 2E). We next created nuclear and cell outline meshes by applying MorphoGraphX-based segmentation on the z stacks (Figure 2F) and defined cellular (CC) and nuclear centroid (NC) to calculate nuclear position relative to the centroid of the cell. Defining a central axis through the suspensor, we could measure absolute distance of NC to CC, as well as its displacement in longitudinal and radial directions (Figure 2G). For both 4-cell and 8-cell embryos, we could not find significant differences in nuclear position between wild-type and *RPS5A>>bdl* mutant embryos (Figure 2H). Interestingly, we found considerable variation in nuclear position even in wild-type cells, where the division plane is essentially invariable. These findings suggest that correlation of nuclear position with division plane position is not altered in the *bdl* mutant despite the switch to symmetric division. Additionally, these findings also imply that nuclear position may not be strongly connected to cell division orientation and is perhaps not a mechanism mediating its control in early embryos.

Given that minimal surface area and the cell centroid are defined by cellular shape, a switch to a different cell division plane in auxin-insensitive mutants could also be indirectly caused by altered cell shape. Segmentation analysis of wild-type embryos revealed that cells at the 4-cell stage exhibit higher cell volume and area compared to 8-cell stage (Figure 3A), corroborating our previous observation that early division transitions happen with minimal expansion.[8] *RPS5A>>bdl* mutant embryos in comparison exhibit significantly larger cell volume and wall area at both 4-cell and 8-cell stages (Figure 3A), indicating that cell geometry is indeed affected in the *bdl* mutant. To determine whether the observed cell expansion is random or directed in either of the cellular directions, we measured circumferential, radial, and longitudinal cell lengths of the same embryonic cell volumes (Figure 3B). Although at 4-cell stage, cell length in *RPS5A>>bdl* embryos was slightly increased in comparison to wild-type in all measured directions, elongation in the longitudinal direction is dominant. At the 8-cell stage, the circumferential length is high in wild-type cells, while the radial and longitudinal lengths are similar to each other and lower (Figure 3C). In *bdl* embryos, however, longitudinal cell length is higher and closer to circumferential cell length compared to wild-type. To more directly measure cell shape, we calculated the ratio of radial

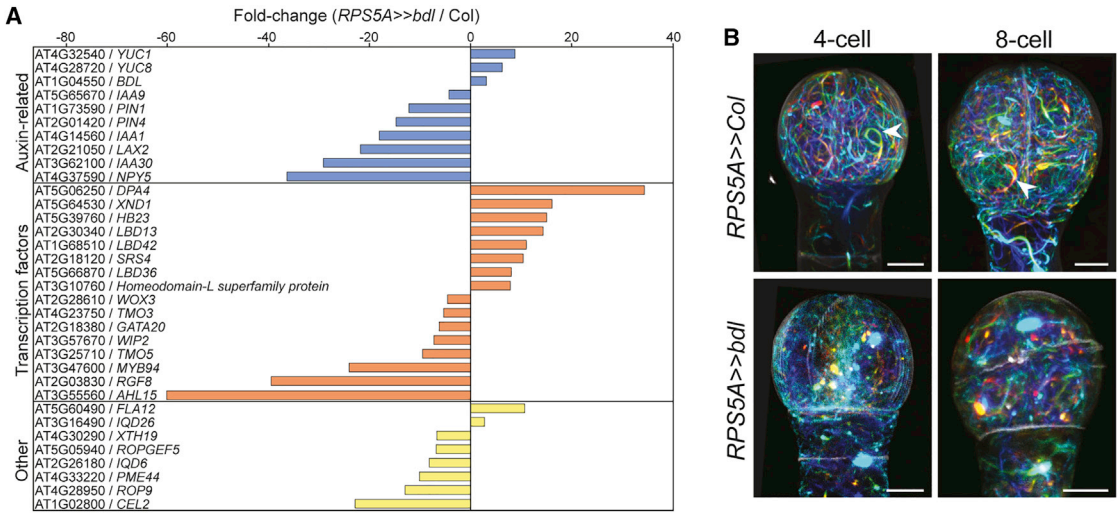

Figure 4. Transcriptome analysis of *RPS5A>>>bdl* embryos

(A) Selected misregulated genes in *bdl* mutant (*RPS5A>>bdl*) 8-cell embryos. Fold-change values are given for expression levels of genes in the *bdl* mutant relative to wild-type (*RPS5A>>*Col).

(B) Maximum projections of depth color-coded F-actin stacks visualized using Lifeact-tdTomato (ACE-W14) reporter. Embryo microtubule mounting (EMTM) solution[22] was used for mounting. Scale bars, 5 μm.

See also Figure S2 and Table S1.

and circumferential cell lengths to the longitudinal cell length. At 4-cell stage, the ratios suggest minimal to no difference between wild-type and *bdl* embryos. In wild-type, 8-cell stage cells show higher radial and circumferential ratios compared to the 4-cell stage (Figure 3D), revealing obvious but significant cell shape changes during the 4- to 8-cell transition. In contrast, both ratios of *bdl* embryos at 8-cell stage are significantly lower in comparison to wild-type, indicating abnormal expansion defects in *bdl* embryos do lead to cell shape irregularities. Detailed analysis of cells in the upper (apical) and lower (basal) tier of the embryo revealed that shape defects in mutant cells are found in both tiers. In addition, the distinction in shape between apical and basal cells is reduced in *RPS5A>>bdl* embryos (Figures 3E and S1). Hence, this analysis shows that the altered cell division planes are preceded by changes in cell geometry, suggesting that the primary target of auxin control could be a process that controls cell shape.

Transcriptome analysis reveals altered cytoskeletal gene expression

To probe the genetic mechanisms underlying auxin-dependent cell expansion and division plane orientation, we performed transcriptome analysis, comparing manually isolated 8-cell wild-type and *RPS5A>>bdl* mutant embryos. Given that the molecular target of bdl is ARF-dependent transcriptional control, the immediate cellular pathways that are subject to auxin regulation should be apparent from the genes misregulated. We chose the 8-cell stage, as this represents the moment shortly before the switch in division orientation . Initial inspection of the *RPS5A>>bdl* transcriptome revealed the expected upregulation of *BDL/IAA12* while other *Aux/IAA* genes were downregulated (Figure S2A), consistent with genome-wide dampening of auxin response. Additionally, 5 out of 11 *YUC* genes were upregulated in *bdl* embryos (Figure S2A), which shows that also auxin-dependent gene repression is inhibited in mutant embryos and validates the effectiveness of the inhibition of auxin response. After statistical analysis, we retained 421 up- and 414 downregulated genes in *RPS5A>>bdl* embryos (>2-fold difference; q value < 0.05; Table S1). Gene Ontology (GO) analysis did not identify obvious enrichment of functional categories. Nevertheless, among the highly misexpressed genes, we found several genes involved in cellular mechanisms, along with known developmental regulators. Here, we focus on 34 candidate genes that could be divided into three groups based on their ontology information and functional data from earlier studies (Figure 4A). The first group represents genes related to auxin signaling (*IAA1*, *IAA9*, and *IAA30*), biosynthesis (*YUC1* and *YUC8*), and transport (*PIN1*, *PIN4*, *LAX2*, and *NPY5*). The second group includes transcription factors, of which most are known to be key regulators of development, including several known auxin response targets (e.g., *TMO3*, *GATA20*, *WIP2*, and *TMO5*). The third group contained genes known for their function in cytoskeletal organization and signaling, along with genes involved in cell wall composition and remodeling. A pectin methyl esterase (*PME44*), xyloglucan endotransglycosylase (*XTH19*), cellulase (*CEL2*), and an arabinogalactan protein (*FLA12*) were found downregulated in *bdl* embryos. All these are known for their roles in cell wall remodeling mechanisms during post-embryonic growth. We found significant downregulation of the ROP-activating guanine exchange factor, *ROP-GEF5*, along with *ROP9*, which belongs to type II sub-group of *ROP* gene family. The plant-specific small Rho guanosine triphosphatase (GTPase) switches, ROPs, are known for their function in tip-growing cells like pollen tube and root hair cells as well as interdigitating epidermal pavement cells by regulating actin-microtubule (MT) dynamics.[24,25] Conversion from the inactive guanosine diphosphate (GDP)- to active GTP-bound

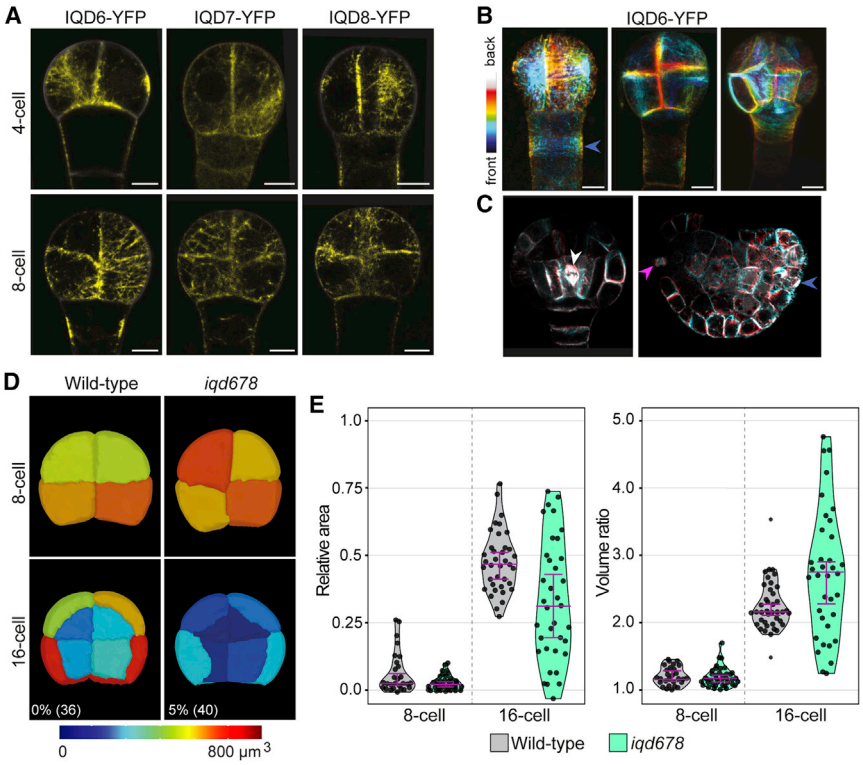

Figure 5. IQD6 mediates auxin response in embryonic division plane control

(A) *IQDX$_{pro}$:IQDX-sYFP* reporter lines show strand-like structures resembling microtubules.

(B) Depth color-coded IQD6-sYFP stacks of 4-, 8-, and 16-cell embryos show localization of protein in 3D.

(C) 3D representation of two successive confocal sections of IQD6-sYFP in late embryos. Arrowheads indicate observed localization in pre-prophase bands (PPBs) (blue), spindle (white), and phragmoplast (magenta). EMTM solution[22] was used for mounting the embryos.

(D) 3D embryo phenotype of wild-type and *iqd678* mutant embryos with cell colors corresponding to cellular volume (in µm^3) indicated in the color scale. The percentage of symmetric orientation defects at 16-cell stage and number of cell pairs analyzed (% (n)) are indicated at the bottom.

(E) Violin plots representing distribution of division plane areas and volume ratios as described in Figure 1B. At least 5 individual embryos were used per condition.

See also Figures S3 and S4.

form of ROPs is triggered by ROP-GEFs.[26] Additionally, two IQ67 domain (*IQD*) family genes *IQD6* and *IQD18* were also found downregulated in the *RPS5A>>bdl* background. IQD proteins interact with calmodulin (CaM) signaling modules and are proposed to mediate Ca^{2+}-dependent regulation of MT organization and dynamics.[27,28] IQD proteins are also emerging as key components in ROP signaling by regulating plasma membrane-MT dynamics for localized growth alterations.[29]

Auxin response controls cytoskeleton organization in the embryo

The altered expression of a set of genes encoding regulators of actin and MT cytoskeleton function in auxin-insensitive *RPS5A>>bdl* embryos suggests that auxin response controls these two cytoskeletal structures. We have previously demonstrated that length and degree of MT polymerization is reduced in *RPS5A>>bdl* embryos, and modeling suggested this to contribute to choice of division plane.[30] To address whether actin organization is also altered, we introduced a *WOX2$_{pro}$:LifeAct-tdTomato* (ACE-W14) marker into the *RPS5A>>bdl* background. Previously, we reported thick F-actin bundles in early embryonic cells, which form arches around the nucleus (Figure 4B).[22] These thick actin bundles were absent in *RPS5A>>bdl* cells (Figure S2B), and in addition, we observed loss of dense F-actin meshwork in mutant cells (Figure 4B). Quantification revealed a strong increase in cytosolic LifeAct-tdTomato signal in *RPS5A>>bdl* embryos (Figure S2C). Thus, in addition to the effects on the MT cytoskeleton, impaired auxin response causes a disruption of the actin cytoskeleton in the embryo. By inference, auxin controls the organization of both cytoskeletal structures.

Auxin-dependent, MT-associated IQD6 functions in division control

It is likely that the influence on cytoskeleton function that auxin exerts is mediated by the genes identified as being downregulated in *RPS5A>>bdl* embryos. Here, we focused on the *IQD6* gene, which was strongly downregulated (Figure 4A). Previously, inhibition of auxin response on other developmental contexts had been shown to affect the expression of several *IQD* family members.[31–34] Indeed, apart from *IQD6* and *IQD18*, we also observed downregulation of several *IQD* family genes in the *RPS5A>>bdl* mutant background (Figure S3A). We first determined the subcellular localization of IQD6 protein, as well as its close homologs IQD7 and IQD8, by generating C-terminal fusions with YFP (*IQDX$_{pro}$:IQDX-sYFP*). All three proteins show broad accumulation in embryos and roots, with IQD6 and 7 showing a slight enrichment in the root vasculature (Figures 5A, S4A, and S4B). All three IQD proteins exhibited filamentous localization near cell membranes in early embryonic stages, strongly resembling the cortical MT localization reported for embryos previously. IQD6/7/8 proteins localized to the mitotic spindle, phragmoplast, and PPB (Figures 5B, 5C, and S4C), which was not observed for previously reported IQD protein subclades,[33] suggesting a possibility of different function for the IQD6–8 family subclade.

To investigate the involvement of IQD6, 7, and 8 in division plane orientation, we analyzed the embryos of *iqd678* triple mutants. This mutant was recently reported to have distorted cell division planes in roots, along with alterations in the organization of the MT cytoskeleton.[35] Likewise, in 35% of the analyzed embryos (Figure S3B), the mutant shows a shift in division plane orientation during different stages, which varies from subtle to more severe defects (Figure S3C). The divisions leading to 8-cell embryos are symmetric and use the minimal surface area, similar to wild-type embryos (Figures 5D and 5E). In contrast, the divisions leading to 16-cell embryos show a high

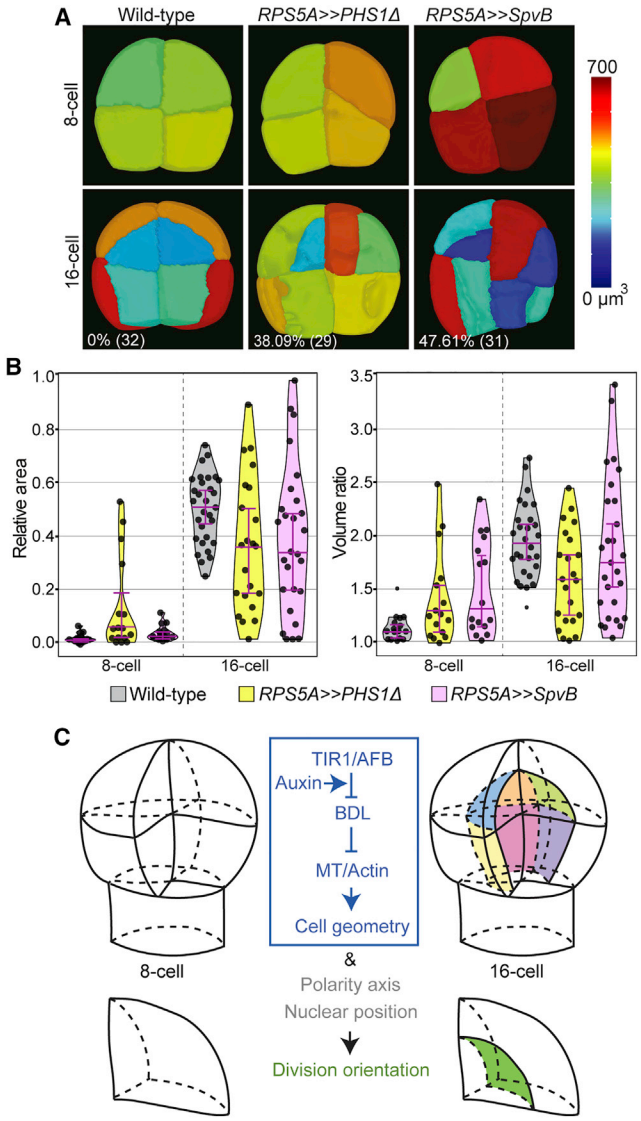

Figure 6. Genetic perturbation of MT and actin cytoskeleton inhibits asymmetric embryonic divisions

(A) 3D comparison of wild-type, *RPS5A>>PHS1Δ*, and *RPS5A>>SpvB*-mutant embryos. Cell colors correspond to cellular volume as indicated in the color scale. The percentage of symmetric orientation defects at 16-cell stage and number of cell pairs analyzed (% (n)) are indicated at the bottom.

(B) Violin plots representing distribution of division plane areas and volume ratios, as described in Figure 1B. At least 4 individual embryos were used per condition.

(C) Model depicting how auxin controls division orientation. Auxin influences cytoskeleton dynamics and organization, thus regulating cell shape. Along with polarity and nuclear position, this defines the cell division plane.

See also Figures S5 and S6.

degree of division plane area variation, with values spanning across and beyond the relative areas of wild-type 8-cell and 16-cell stages (Figures 5D and 5E). Consequently, volume distribution ratios are also highly variable, from wild-type-like asymmetric divisions to highly symmetric divisions with volume ratios smaller than *RPS5A>>bdl* mutant embryos (Figures 1B and 5E). Nevertheless, the *iqd678* mutant embryos do not show the severe *bdl*-like division phenotype (Figure 5D). These results suggest that IQD6–8 proteins are involved in cell division placement. However, the variability in division plane parameters indicate that this function is not absolute and may signify the involvement of other IQD proteins or additional components.

Both MT and actin cytoskeletons contribute to regulated division plane orientation

Disruption of MT and actin cytoskeleton is correlated with altered cell division planes in *RPS5A>>bdl* embryos, and this is in turn coupled to altered expression of genes encoding cytoskeletal regulators. It is thus likely that cytoskeleton organization contributes causally to division plane choice in embryo cells. If this were the case, one would expect direct interference with either cytoskeleton to alter cell division planes. Prolonged treatments with cytoskeleton-destabilizing or stabilizing drugs in embryos are not trivial and require *in vitro* culturing of seeds, which in itself can cause abnormalities.[36] We therefore made use of genetic tools to depolymerize MT or F-actin filaments by expression of the PHS1Δ (MT)[37] or SpvB (actin)[38] proteins. Expression of these proteins was previously shown to be equivalent to treatment with MT- or actin-depolymerizing drugs and disrupts asymmetric radial expansion and polar migration of nuclei in lateral root founder cells.[10] We generated fluorescently tagged versions of PHS1Δ (mNeonGreen-PHS1Δ) and SpvB (SpvB-mNeonGreen) and used *GAL4-UAS* two-component gene expression to drive their expression in embryos only after fertilization, driven by the *RPS5A* promoter. Expression of both proteins in embryos caused frequent changes in division planes. MT depolymerization through PHS1Δ expression led to defects in 95% of embryos (n = 122) and caused oblique divisions (Figures 6A and S5) that superficially resemble those induced by inhibition of auxin response. Depolymerizing actin through SpvB expression led to essentially indistinguishable defects in 85% of embryos (n = 165). Also, here, altered division planes are similar to those observed in *RPS5A>>bdl* and *tir1afb12345* embryos (Figures 6A and S5). Defects were obvious at all stages analyzed (Figures 6A and S5). While wall area and cell volume ratio were more variable than in wild-type at 8-cell stage (Figures 6B and S6), there was no consistent switch to altered division plane. At 16-cell stage, the asymmetry and volume distribution among cells were also more variable than in wild-type (Figure 6B). In a small number of cells, division wall surface area was larger than in wild-type, correlating with a small population of cells with more asymmetric division (Figure 6B). At the same time, a larger fraction of cells show *bdl*-like orientation defects (Figure 6A), leading to smaller division wall surface area and thus overall lower average value in both *RPS5A>>PHS1Δ* and *RPS5A>>SpvB* embryos (Figure 6B). Consequently, division asymmetry was also reduced in both transgenic genotypes. Thus, while depolymerization of both cytoskeletons expectedly caused more pleiotropic defects in cell division plane orientation, these defects include the switch to smaller division wall surface area and loss of asymmetric division. We therefore conclude that regulation of the MT and actin cytoskeleton is critical for asymmetric cell division in the early *Arabidopsis* embryo and that auxin response may indeed regulate division orientation through its effects on the cytoskeleton.

DISCUSSION

Combining embryo-specific fluorescent cellular reporters with 3D imaging and cell segmentation, we analyzed the role of early polarity axis, nuclear position, cell shape, and auxin-mediated cytoskeleton dynamics in orienting the division plane in early embryos. Surprisingly, despite nearly invariant division planes, nucleus position was found to be variable, even in wild-type. Unless we missed a transient stabilization of nuclear position just prior to mitosis, this finding suggests that nuclear position is not instructive for positioning the division plane in early embryo cells. What is evident though is that changes in cell shape between wild-type and auxin-insensitive embryos correlate with altered division planes. This identifies the control of cell shape as a mediator of division plane choice (Figure 6C). While cell wall biology is complex and multifactorial, a key influence on cell shape is the deposition of cellulose fibers along tracks that are dictated by the CMT filaments. Thus, MTs dictate the pattern of cell wall fortification and thereby constrain and bias directional elongation, resulting in cell shape changes.[39] Using markers for MT and actin, we show that the organization of both is subject to auxin-dependent regulation. This finding is consistent with their central role in post-embryonic division orientation control.[40,41] We identified auxin-dependent genes with known functions in cytoskeleton reorganization. Characterization of IQD6 and its family members imply a significant role in orienting the division plane. While we did not explore other auxin-dependent genes here, several link to the processes identified to be critical to division orientation. First, a ROP11-IQD13 signaling module was found important for localized growth changes in the formation of xylem pits by organizing CMTs.[29] ROPs are well known to regulate cytoskeleton dynamics during tip growth and in pavement cell interdigitation.[42] CMT stability and polymerization dynamics regulate the PPB formation.[43,44] Simulation studies of CMTs on segmented embryonic cell shapes identify transient auxin-mediated CMT stabilization as a plausible mechanism in division plane orientation.[30] Thus, ROP-mediated cytoskeleton dynamics may play a critical role in keeping the homeostasis of CMTs and fine-tuning of the PPB for asymmetric orientation. Second, the identification of a set of cell-wall-related enzymes suggests that auxin regulation may also directly control wall biochemistry. Recent work has revealed the significance of pectin and xyloglucan in cell wall integrity and remodeling. Methyl esterification status of pectin determines the plasticity of the cell wall, and defects lead to severe phenotypes in post-embryonic tissues.[45] These studies represent the wall reorganization effects at tissue and organ level, but our current knowledge about PME or XTH wall remodeling in confined cellular mechanisms like division plane orientation remains poor. The current study opens new avenues for answering these intriguing questions.

We show that outside-inside cell polarity establishment is independent of transcriptional auxin response. Thus, unless the outside-inside polarity system has multiple (auxin-dependent and independent) branches, auxin acts to control division downstream of this polarity axis. Because no regulators of this axis with function in the embryo have yet been identified, it is at present unknown how this polarity axis still biases the choice of the division plane, and it will be interesting to see how this interacts with the auxin-dependent control of cytoskeleton dynamics and cell shape. Recently, we identified a family of SOSEKI polarity proteins, of which two members are transcriptionally controlled by auxin response.[46] Thus, at least part of the polarity system is dependent on auxin input. Misexpression of the SOSEKI1 protein causes oblique cell divisions, suggesting a link to the division orientation machinery. However, it is equally likely that SOSEKI1 affects the CMT or cell shape and only indirectly influences division plane. Further investigation of this protein family should help resolve how the different cell polarity systems are linked to division control in the embryo.

STAR★METHODS

Detailed methods are provided in the online version of this paper and include the following:

- KEY RESOURCES TABLE
- RESOURCE AVAILABILITY
  - Lead contact
  - Materials availability
  - Data and code availability
- EXPERIMENTAL MODEL AND SUBJECT DETAILS
  - Plant Material and Growth Conditions
- METHOD DETAILS
  - Molecular cloning
  - Generation and selection of transgenic plants
  - Microscopy and image analysis
  - 3D cell segmentation and nuclear position measurements
  - 3D cell morphology measurements
  - Shortest division plane estimation and comparison to actual division plane
  - Embryo isolation and transcriptome analysis
- QUANTIFICATION AND STATISTICAL ANALYSIS

SUPPLEMENTAL INFORMATION

Supplemental information can be found online at https://doi.org/10.1016/j.cub.2021.09.019.

ACKNOWLEDGMENTS

The authors are grateful to Mark Estelle and Michael Prigge (UCSD) for sharing the *tir1 afb* hextuple mutant, to Alexis Maizel for sharing template plasmids for PHS1Δ and SpvB constructs, and to Valentijn Jansen, Joakim Palovaara, Jenny Jansen, and Mark Boekschoten for help and support with initial transcriptome analysis and data analysis. This work was funded by a fellowship from the German funding agency (DFG; VA 1156/1-1 and VA 1156/2-1) to P.V. and grants from the Netherlands Organization for Scientific Research (NWO) (ALW Open Competition grant 824.14.009) and the European Research Council (starting grant "CELLPATTERN," contract number 281573; advanced grant "DIRNDL," contract number 833867) to D.W.

AUTHOR CONTRIBUTIONS

Conceptualization, P.V., T.d.Z., and D.W.; investigation, P.V., T.d.Z., S.S., C.-Y.L., and J.J.R.; resources, K.B.; formal analysis, P.V., T.d.Z., and S.S.; software and methodology, S.S. and R.S.S.; supervision, R.S.S. and D.W.; funding acquisition, P.V. and D.W.; writing – original draft, P.V.; writing – review & editing, P.V. and D.W. with input from all the authors.

DECLARATION OF INTERESTS

The authors declare no competing interests.

Received: February 9, 2021
Revised: July 22, 2021
Accepted: September 7, 2021
Published: October 4, 2021

REFERENCES

1. Errera, L. (1888). Uber zellformen und seifenblasen. Bot. Zentralbl. *34*, 395–398.
2. Sachs, J. (1878). Über die anordnung der zellen in jungsten pflanzenteilen. Arb. Bot. Inst. Würzburg *2*, 46–104.
3. Hofmeister, W. (1863). Zusatze und berichtigungen zu den 1851 veroffentlichten untersuchungen der entwicklung hoherer krytogamen. Jahrb. Wiss. Bot. *3*, 259–293.
4. Torres-Ruiz, R.A., and Jürgens, G. (1994). Mutations in the FASS gene uncouple pattern formation and morphogenesis in Arabidopsis development. Development *120*, 2967–2978.
5. Friml, J., Vieten, A., Sauer, M., Weijers, D., Schwarz, H., Hamann, T., Offringa, R., and Jürgens, G. (2003). Efflux-dependent auxin gradients establish the apical-basal axis of Arabidopsis. Nature *426*, 147–153.
6. Wendrich, J.R., and Weijers, D. (2013). The Arabidopsis embryo as a miniature morphogenesis model. New Phytol. *199*, 14–25.
7. Besson, S., and Dumais, J. (2011). Universal rule for the symmetric division of plant cells. Proc. Natl. Acad. Sci. USA *108*, 6294–6299.
8. Yoshida, S., Barbier de Reuille, P., Lane, B., Bassel, G.W., Prusinkiewicz, P., Smith, R.S., and Weijers, D. (2014). Genetic control of plant development by overriding a geometric division rule. Dev. Cell *29*, 75–87.
9. Kimata, Y., Higaki, T., Kawashima, T., Kurihara, D., Sato, Y., Yamada, T., Hasezawa, S., Berger, F., Higashiyama, T., and Ueda, M. (2016). Cytoskeleton dynamics control the first asymmetric cell division in Arabidopsis zygote. Proc. Natl. Acad. Sci. USA *113*, 14157–14162.
10. Vilches Barro, A., Stöckle, D., Thellmann, M., Ruiz-Duarte, P., Bald, L., Louveaux, M., von Born, P., Denninger, P., Goh, T., Fukaki, H., et al. (2019). Cytoskeleton dynamics are necessary for early events of lateral root initiation in Arabidopsis. Curr. Biol. *29*, 2443–2454.e5.
11. Shao, W., and Dong, J. (2016). Polarity in plant asymmetric cell division: division orientation and cell fate differentiation. Dev. Biol. *419*, 121–131.
12. Murata, T., and Wada, M. (1991). Effects of centrifugation on preprophase-band formation in Adiantum protonemata. Planta *183*, 391–398.
13. Muroyama, A., Gong, Y., and Bergmann, D.C. (2020). Opposing, polarity-driven nuclear migrations underpin asymmetric divisions to pattern Arabidopsis stomata. Curr. Biol. *30*, 4467–4475.e4.
14. Scheres, B., Wolkenfelt, H., Willemsen, V., Terlouw, M., Lawson, E., Dean, C., and Weisbeek, P. (1994). Embryonic origin of the Arabidopsis primary root and root meristem initials. Development *120*, 2475–2487.
15. Jürgens, G., and Mayer, U. (1994). Arabidopsis. In Embryos: Color Atlas of Development, , J. Bard, ed. (Wolfe), pp. 7–21.
16. Rademacher, E.H., Lokerse, A.S., Schlereth, A., Llavata-Peris, C.I., Bayer, M., Kientz, M., Freire Rios, A., Borst, J.W., Lukowitz, W., Jürgens, G., and Weijers, D. (2012). Different auxin response machineries control distinct cell fates in the early plant embryo. Dev. Cell *22*, 211–222.
17. Moukhtar, J., Trubuil, A., Belcram, K., Legland, D., Khadir, Z., Urbain, A., Palauqui, J.-C., and Andrey, P. (2019). Cell geometry determines symmetric and asymmetric division plane selection in Arabidopsis early embryos. PLoS Comput. Biol. *15*, e1006771.
18. Roosjen, M., Paque, S., and Weijers, D. (2018). Auxin response factors: output control in auxin biology. J. Exp. Bot. *69*, 179–188.
19. Hamann, T., Benkova, E., Bäurle, I., Kientz, M., and Jürgens, G. (2002). The Arabidopsis BODENLOS gene encodes an auxin response protein inhibiting MONOPTEROS-mediated embryo patterning. Genes Dev. *16*, 1610–1615.
20. Prigge, M.J., Platre, M., Kadakia, N., Zhang, Y., Greenham, K., Szutu, W., Pandey, B.K., Bhosale, R.A., Bennett, M.J., Busch, W., and Estelle, M. (2020). Genetic analysis of the Arabidopsis TIR1/AFB auxin receptors reveals both overlapping and specialized functions. eLife *9*, e54740.
21. Barbier de Reuille, P., Routier-Kierzkowska, A.-L., Kierzkowski, D., Bassel, G.W., Schüpbach, T., Tauriello, G., Bajpai, N., Strauss, S., Weber, A., Kiss, A., et al. (2015). MorphoGraphX: a platform for quantifying morphogenesis in 4D. eLife *4*, 05864.
22. Liao, C.Y., and Weijers, D. (2018). A toolkit for studying cellular reorganization during early embryogenesis in Arabidopsis thaliana. Plant J. *93*, 963–976.
23. Robinson, S., Barbier de Reuille, P., Chan, J., Bergmann, D., Prusinkiewicz, P., and Coen, E. (2011). Generation of spatial patterns through cell polarity switching. Science *333*, 1436–1440.
24. Feiguelman, G., Fu, Y., and Yalovsky, S. (2018). ROP GTPases structure-function and signaling pathways. Plant Physiol. *176*, 57–79.
25. Yang, Z., and Fu, Y. (2007). ROP/RAC GTPase signaling. Curr. Opin. Plant Biol. *10*, 490–494.
26. Gu, Y., Li, S., Lord, E.M., and Yang, Z. (2006). Members of a novel class of Arabidopsis Rho guanine nucleotide exchange factors control Rho GTPase-dependent polar growth. Plant Cell *18*, 366–381.
27. Bürstenbinder, K., Savchenko, T., Müller, J., Adamson, A.W., Stamm, G., Kwong, R., Zipp, B.J., Dinesh, D.C., and Abel, S. (2013). Arabidopsis calmodulin-binding protein IQ67-domain 1 localizes to microtubules and interacts with kinesin light chain-related protein-1. J. Biol. Chem. *288*, 1871–1882.
28. Bürstenbinder, K., Möller, B., Plötner, R., Stamm, G., Hause, G., Mitra, D., and Abel, S. (2017). The IQD family of calmodulin-binding proteins links calcium signaling to microtubules, membrane subdomains, and the nucleus. Plant Physiol. *173*, 1692–1708.
29. Sugiyama, Y., Wakazaki, M., Toyooka, K., Fukuda, H., and Oda, Y. (2017). A novel plasma membrane-anchored protein regulates xylem cell-wall deposition through microtubule-dependent lateral inhibition of Rho GTPase domains. Curr. Biol. *27*, 2522–2528.e4.
30. Chakrabortty, B., Willemsen, V., de Zeeuw, T., Liao, C.-Y., Weijers, D., Mulder, B., and Scheres, B. (2018). A plausible microtubule-based mechanism for cell division orientation in plant embryogenesis. Curr. Biol. *28*, 3031–3043.e2.
31. Schlereth, A., Möller, B., Liu, W., Kientz, M., Flipse, J., Rademacher, E.H., Schmid, M., Jürgens, G., and Weijers, D. (2010). MONOPTEROS controls embryonic root initiation by regulating a mobile transcription factor. Nature *464*, 913–916.
32. Möller, B.K., ten Hove, C.A., Xiang, D., Williams, N., López, L.G., Yoshida, S., et al. (2017). Auxin response cell-autonomously controls ground tissue initiation in the early *Arabidopsis* embryo. Proc. Natl. Acad. Sci. USA *114*, E2533–E2539.
33. Wendrich, J.R., Yang, B.-J., Mijnhout, P., Xue, H.-W., Rybel, B.D., and Weijers, D. (2018). IQD proteins integrate auxin and calcium signaling to regulate microtubule dynamics during Arabidopsis development. bioRxiv. https://doi.org/10.1101/275560.
34. Wendrich, J.R., Möller, B.K., Li, S., Saiga, S., Sozzani, R., Benfey, P.N., De Rybel, B., and Weijers, D. (2017). Framework for gradual progression of cell ontogeny in the *Arabidopsis* root meristem. Proc. Natl. Acad. Sci. USA *114*, E8922–E8929.
35. Kumari, P., Dahiya, P., Livanos, P., Zergiebel, L., Kölling, M., Poeschl, Y., Stamm, G., Hermann, A., Abel, S., Müller, S., and Bürstenbinder, K. (2021). IQ67 DOMAIN proteins facilitate preprophase band formation and division-plane orientation. Nat. Plants *7*, 739–747.
36. Sauer, M., and Friml, J. (2004). In vitro culture of Arabidopsis embryos within their ovules. Plant J. *40*, 835–843.
37. Fujita, S., Pytela, J., Hotta, T., Kato, T., Hamada, T., Akamatsu, R., Ishida, Y., Kutsuna, N., Hasezawa, S., Nomura, Y., et al. (2013). An atypical tubulin

kinase mediates stress-induced microtubule depolymerization in Arabidopsis. Curr. Biol. *23*, 1969–1978.

38. Harterink, M., da Silva, M.E., Will, L., Turan, J., Ibrahim, A., Lang, A.E., van Battum, E.Y., Pasterkamp, R.J., Kapitein, L.C., Kudryashov, D., et al. (2017). DeActs: genetically encoded tools for perturbing the actin cytoskeleton in single cells. Nat. Methods *14*, 479–482.
39. Szymanski, D.B., and Cosgrove, D.J. (2009). Dynamic coordination of cytoskeletal and cell wall systems during plant cell morphogenesis. Curr. Biol. *19*, R800–R811.
40. Rasmussen, C.G., Wright, A.J., and Müller, S. (2013). The role of the cytoskeleton and associated proteins in determination of the plant cell division plane. Plant J. *75*, 258–269.
41. Li, S., Sun, T., and Ren, H. (2015). The functions of the cytoskeleton and associated proteins during mitosis and cytokinesis in plant cells. Front. Plant Sci. *6*, 282.
42. Fu, Y., Li, H., and Yang, Z. (2002). The ROP2 GTPase controls the formation of cortical fine F-actin and the early phase of directional cell expansion during Arabidopsis organogenesis. Plant Cell *14*, 777–794.
43. Dhonukshe, P., and Gadella, T.W.J., Jr. (2003). Alteration of microtubule dynamic instability during preprophase band formation revealed by yellow fluorescent protein-CLIP170 microtubule plus-end labeling. Plant Cell *15*, 597–611.
44. Vos, J.W., Dogterom, M., and Emons, A.M.C. (2004). Microtubules become more dynamic but not shorter during preprophase band formation: a possible "search-and-capture" mechanism for microtubule translocation. Cell Motil. Cytoskeleton *57*, 246–258.
45. Wolf, S., Mravec, J., Greiner, S., Mouille, G., and Höfte, H. (2012). Plant cell wall homeostasis is mediated by brassinosteroid feedback signaling. Curr. Biol. *22*, 1732–1737.
46. Yoshida, S., van der Schuren, A., van Dop, M., van Galen, L., Saiga, S., Adibi, M., Möller, B., Ten Hove, C.A., Marhavy, P., Smith, R., et al. (2019). A SOSEKI-based coordinate system interprets global polarity cues in Arabidopsis. Nat. Plants *5*, 160–166.
47. Weijers, D., Van Hamburg, J.-P., Van Rijn, E., Hooykaas, P.J.J., and Offringa, R. (2003). Diphtheria toxin-mediated cell ablation reveals interregional communication during Arabidopsis seed development. Plant Physiol. *133*, 1882–1892.
48. Weijers, D., Schlereth, A., Ehrismann, J.S., Schwank, G., Kientz, M., and Jürgens, G. (2006). Auxin triggers transient local signaling for cell specification in Arabidopsis embryogenesis. Dev. Cell *10*, 265–270.
49. Schindelin, J., Arganda-Carreras, I., Frise, E., Kaynig, V., Longair, M., Pietzsch, T., Preibisch, S., Rueden, C., Saalfeld, S., Schmid, B., et al. (2012). Fiji: an open-source platform for biological-image analysis. Nat. Methods *9*, 676–682.
50. R Developmemt Core Team (2017). R: a language and environment for statistical computing (R Foundation for Statistical Computing). https://www.R-project.org/.
51. Murashige, T., and Skoog, F. (1962). A revised medium for rapid growth and bio assays with tobacco tissue cultures. Physiol. Plant. *15*, 473–497.
52. De Rybel, B., van den Berg, W., Lokerse, A., Liao, C.-Y., van Mourik, H., Möller, B., Peris, C.L., and Weijers, D. (2011). A versatile set of ligation-independent cloning vectors for functional studies in plants. Plant Physiol. *156*, 1292–1299.
53. Clough, S.J., and Bent, A.F. (1998). Floral dip: a simplified method for Agrobacterium-mediated transformation of Arabidopsis thaliana. Plant J. *16*, 735–743.
54. Kerstens, M., Strauss, S., Smith, R., and Willemsen, V. (2020). From stained plant tissues to quantitative cell segmentation analysis with MorphoGraphX. Methods Mol. Biol. *2122*, 63–83.
55. Montenegro-Johnson, T.D., Stamm, P., Strauss, S., Topham, A.T., Tsagris, M., Wood, A.T.A., Smith, R.S., and Bassel, G.W. (2015). Digital single-cell analysis of plant organ development using 3DCellAtlas. Plant Cell *27*, 1018–1033.
56. Raissig, M.T., Gagliardini, V., Jaenisch, J., Grossniklaus, U., and Baroux, C. (2013). Efficient and rapid isolation of early-stage embryos from Arabidopsis thaliana seeds. J. Vis. Exp. 50371.
57. Lin, K., Kools, H., de Groot, P.J., Gavai, A.K., Basnet, R.K., Cheng, F., Wu, J., Wang, X., Lommen, A., Hooiveld, G.J.E.J., et al. (2011). MADMAX - management and analysis database for multiple ~omics experiments. J. Integr. Bioinform. *8*, 160.
58. Dai, M., Wang, P., Boyd, A.D., Kostov, G., Athey, B., Jones, E.G., Bunney, W.E., Myers, R.M., Speed, T.P., Akil, H., et al. (2005). Evolving gene/transcript definitions significantly alter the interpretation of GeneChip data. Nucleic Acids Res. *33*, e175.
59. Irizarry, R.A., Hobbs, B., Collin, F., Beazer-Barclay, Y.D., Antonellis, K.J., Scherf, U., and Speed, T.P. (2003). Exploration, normalization, and summaries of high density oligonucleotide array probe level data. Biostatistics *4*, 249–264.
60. Phipson, B., Lee, S., Majewski, I.J., Alexander, W.S., and Smyth, G.K. (2016). Robust hyperparameter estimation protects against hypervariable genes and improves power to detect differential expression. Ann. Appl. Stat. *10*, 946–963.
61. Sartor, M.A., Tomlinson, C.R., Wesselkamper, S.C., Sivaganesan, S., Leikauf, G.D., and Medvedovic, M. (2006). Intensity-based hierarchical Bayes method improves testing for differentially expressed genes in microarray experiments. BMC Bioinformatics *7*, 538.
62. Storey, J.D., and Tibshirani, R. (2003). Statistical significance for genome-wide studies. Proc. Natl. Acad. Sci. USA *100*, 9440–9445.
63. Postma, M., and Goedhart, J. (2019). PlotsOfData-A web app for visualizing data together with their summaries. PLoS Biol. *17*, e3000202.

STAR★METHODS

KEY RESOURCES TABLE

REAGENT or RESOURCE	SOURCE	IDENTIFIER
Chemicals, peptides, and recombinant proteins		
SCRI Renaissance Stain 2200	Renaissance Chemicals	SR2200
Propidium Iodide	Sigma-Aldrich	Cat#P4170
Paclitaxel, 99+%, ACROS Organics	Fisherscientific	Cat#33069-62-4
Plant Agar	Duchefa	Cat#P1001.1000
Phosphinotricin	Duchefa	Cat#P0159.1000
Kanamycin (Sulfate Munohydrate)	Duchefa	Cat#K0126.0010
Critical commercial assays		
Ovation Pico WTA System V2	Nugen	Cat#3302-12
Deposited data		
Microarray	This study	GEO: GSE165986
Experimental models: organisms/strains		
Arabidopsis thaliana accession Col-0	Widely distributed	N/A
Arabidopsis: tir1/afb hexuple mutant	Prigge et al.[20]	N/A
Arabidopsis: $RPS5A_{pro}$:GAL4-VP16	Weijers et al.[47]	RPS5A-GAL4
Arabidopsis: UAS_{pro}:bdl	Weijers et al.[48]	UAS-bdl
Arabidopsis: $WOX2_{pro}$:BOR1-mCitrine	Liao and Weijers[22]	ACE-W03
Arabidopsis: $WOX2_{pro}$:AtNUP54-GFP	Liao and Weijers[22]	ACE-W11
Arabidopsis: $WOX2_{pro}$:Lifeact-tdTomato	Liao and Weijers[22]	ACE-W14
Arabidopsis: $IQD6_{pro}$:IQD6-sYFP	This study	N/A
Arabidopsis: $IQD7_{pro}$:IQD7-sYFP	This study	N/A
Arabidopsis: $IQD8_{pro}$:IQD8-sYFP	This study	N/A
Arabidopsis: UAS_{pro}:PHS1ΔP-mNeonGreen	This study	N/A
Arabidopsis: UAS_{pro}:mNeonGreen-SpvB	This study	N/A
Oligonucleotides		
For primers used see Table S1	N/A	N/A
Recombinant DNA		
Plasmid: *$IQD6_{pro}$:IQD6-sYFP*	This study	N/A
Plasmid: *$IQD7_{pro}$:IQD7-sYFP*	This study	N/A
Plasmid: *$IQD8_{pro}$:IQD8-sYFP*	This study	N/A
Plasmid: *UAS_{pro}:PHS1ΔP-mNeonGreen*	This study	N/A
Plasmid: *UAS_{pro}:mNeonGreen-SpvB*	This study	N/A
Software and algorithms		
Fiji	Schindelin et al.[49]	https://fiji.sc/
MorphoGraphX	Barbier de Reuille et al.[21]	https://www.mpipz.mpg.de/MorphoGraphX
R	R Development Core Team[50]	https://www.r-project.org/

RESOURCE AVAILABILITY

Lead contact

Further information and requests for resources and reagents should be directed to and will be fulfilled by the lead contact, Dolf Weijers (dolf.weijers@wur.nl).

Materials availability

DNA constructs and transgenic *Arabidopsis* seeds generated in this study are available from the lead contact, Dolf Weijers, upon request.

Data and code availability

The transcriptome data have been deposited in the NCBI Gene Expression Omnibus and are accessible through accession number GSE165986. The misregulated genes are listed in Table S1. Microscopy data reported in this paper will be shared by the lead contact upon request.

No new code has been generated in this study.

Any additional information required to reanalyze the data reported in this paper is available from the lead contact upon request.

EXPERIMENTAL MODEL AND SUBJECT DETAILS

Plant Material and Growth Conditions

Arabidopsis ecotype Columbia-0 (Col-0) was used for generating all the transgenic lines. Plants were grown at a constant temperature of 22°C with a 16-hr light/8-hr dark cycle in custom-built growth chambers with light intensity of 110 μE m^{-2} s^{-1}. *Arabidopsis* seeds were surface sterilized using commercial bleach (4% Sodium hypochlorite) and 75% ethanol, followed by washes with 100% ethanol, and were subsequently placed on half-strength Murashige and Skoog (MS) medium[51] with 0.7% plant agar (Duchefa, the Netherlands). After a 48-hour stratification and 10 days of growth on plates, seedlings were transferred to soil. *tir1 afb* hexuple mutant seeds[20] were provided by Mark Estelle and Michael Prigge (UCSD). ACE-W03 (*$WOX2_{pro}$:BOR1-mCitrine*), ACE-W11 (*$WOX2_{pro}$:AtNUP54-GFP*) and ACE-W14 (*$WOX2_{pro}$:Lifeact-tdTomato*) were previously described.[22] For all crosses *RPS5A-GAL4* (*$RPS5A_{pro}$:mGAL4-VP16)*[47] was used as female parent. For *bdl* embryo geometric analysis, F1 seeds of cross between *RPS5A-GAL4* and Col-0 or *UAS-bdl*[48] were used. For nuclear position, F1 seeds of cross between *$WOX2_{pro}$:AtNUP54-GFP* (*RPS5A-GAL4*) and Col-0 or *UAS-bdl* were used. For early polarity analysis, F1 seeds of cross between *$WOX2_{pro}$:BOR1-mCitrine* (*RPS5A-GAL4*) and Col-0 or *UAS-bdl* were used. For F-actin organization, F1 seeds of cross between *$WOX2_{pro}$:Lifeact-tdTomato* (*RPS5A-GAL4*) and Col-0 or *UAS-bdl* were used. For analysis of CMT F1 seeds of cross between *UAS_{pro}:PHS1ΔP-mNeonGreen* and Col-0 or *RPS5A-GAL4* were used.

For analysis of F-actin F1 seeds of cross between *UAS_{pro}:mNeonGreen-SpvB* and Col-0 or *RPS5A-GAL4* were used. Seeds of wild-type (Col-0) and T-DNA insertion lines for *IQD6* (At2g26180, *iqd6*: SALK_137365), *IQD7* (At1g17480, *iqd7*: SALK_025224) and *IQD8* (At1g72670, *iqd8*: SALK_107689) were obtained from the Nottingham *Arabidopsis* Stock Center. All lines were backcrossed at least once with Col-0 and subsequently *iqd6*, *iqd7*, and *iqd8* were crossed among themselves to generate *iqd678* triple mutant.[35]

METHOD DETAILS

Molecular cloning

Plasmids were cloned based on previously described ligation-independent cloning methods and vectors.[52] Whole genomic *IQD-sYFP* fusions were prepared by cloning up to 3kb of promoter including downstream genomic region up to the stop codon into the pPLV117, containing a super Yellow Fluorescent Protein (sYFP). To generate *UAS_{pro}:PHS1ΔP-mNeonGreen* and *UAS_{pro}:mNeonGreen-SpvB* plasmids, *PHS1ΔP-mNeonGreen* and *mNeonGreen-SpvB* sequences were made by overlapping PCR and introduced into HpaI linearized pPLV32. All oligonucleotides used in this study are listed in primer Table S2. IQD-sYFP fusions, *UAS_{pro}:PHS1ΔP-mNeonGreen* and *UAS_{pro}:mNeonGreen-SpvB* were transformed into the Col-0. ACE plasmids[22] were transformed into homozygous *RPS5A-GAL4* (*$RPS5A_{pro}$:GAL4-VP16)* driver line.

Generation and selection of transgenic plants

Transgenic plants were generated by Agrobacterium-mediated floral dip transformation[53] of constructs (see previous section) into backgrounds indicated. Transgenic individuals were selected based on resistance to the appropriate antibiotic or herbicide (15 mg/L phosphinotricin; 50 mg/L kanamycin) on 0,5xMS media, and transplanted to fresh, unsupplemented plates or soil after resistance became apparent. Transgenic lines were analyzed in T2, T3 or T4 generation.

Microscopy and image analysis

Embryos were stained by the modified Pseudo-Schiff propidium iodide (mPS-PI) staining method described in Yoshida et al.[8] with the following modification: An extra treatment with 1% SDS and 0.2 M NaOH for 10 minutes at 37°C was added after fixation. The stained ovules/ embryos were mounted in a drop of chloral hydrate in a well generated by SecureSeal round imaging spacers (20mm, Thermofisher) and observed by confocal microscopy taking z stack images. A series of 2D confocal images were recorded at 0.1 μm intervals using a Leica TCS SP5II confocal laser scanning microscope with a 63 × NA = 1.20 water-immersion objective with pinhole set to 1.0 Airy unit. PI was excited using a diode laser with excitation at 561 nm and detection at 600-700 nm.

Embryo samples were prepared as described in Liao and Weijers.[22] Images for qualitative purpose were acquired in 8-bit format, images for segmentation were acquired in 16-bit format. Images were acquired using a Leica TCS SP5II confocal laser scanning

microscope with 63x NA = 1.2 water objective with pinhole set to 1.0 Airy unit. mGFP and mCitrine were excited by an Argon-ion laser and tdTomato and SCRI Renaissance Stain 2200 (SR2200) (Renaissance Chemicals, http://www.renchem.co.uk/) were excited using a diode laser, and their emissions were detected sequentially with a Leica HyD in photon counting mode. Excitation and detection of fluorophores were configured as follows: mGFP was excited at 488 nm and detected at 498-528 nm; mCitrine was excited at 515nm and detected at 520-540nm tdTomato was excited at 561 nm and detected at 571-630 nm; Renaissance 2200 was excited at 405 nm and detected at 430-470 nm. Line accumulation was set to 4, 4, and 2 for mGFP, tdTomato, and SR2200, respectively. For qualitative results description of F-actin and nuclear structures, maximum projections were generated. For these stacks, background signal outside of the embryo were subtracted, and remaining embryonic signal was multiplied 2-4 times up until signal saturation. For quantification of cytoplasmic Lifeact-tdTomato signal, 4-μm region of interests (ROIs) (n = 30) across the confocal sections from the raw image stack of the embryo were selected randomly for fluorescence intensity measurements. The average tdTomato fluorescence signal intensity was documented and defined as the cytosolic Lifeact-tdTomato signal. 4 to 5 optical sections above the nucleus were used for the selection of ROIs. The optical sections containing the nucleus were not selected for the measurement to avoid interference from the perinuclear actin arches. All image processes and measurements were conducted via Fiji.

3D cell segmentation and nuclear position measurements

For segmentation, in MophoGraphX (MGX),[21] confocal image stacks (TIF) were Gaussian blurred using sigma value 0.6 μm, subsequently we applied the ITK watershed auto-seeding with level threshold value in the range 300–1500 and default smoothing levels. Segmented bitmap stacks were manually corrected for oversegmentation errors within MGX by fusing together multiple labels into the single cells, which were represented using a combination of the select and paint bucket tools in MGX[54] Then, we approximated the segmented cells by creating triangulated surface meshes using marching cubes 3D with cube size of 1. Nuclear measurements were performed on segmented meshes created using the same segmentation method described above using the nuclei marker channel. Cell and nucleus centroid positions were determined in MGX by calculating the center of gravity of their triangulated surface meshes. Organ centric directions were determined in the same way as described in the 3D Cell Atlas Add-on for MGX[55] by manually placing a straight line through the embryo using the "Bezier line" in MGX. For each cell then 3 directions relative to this central line were calculated: a longitudinal direction that is identical with the direction defined by the central line, a radial direction that was defined by the cell centroid and its closest point on the central line, and a circumferential direction that was defined by the cross product of the previous two directions. To calculate the distances between cell centroid and nucleus centroid along the longitudinal and radial direction, the scalar product of the vector defined by the centroids and the vector of the respective direction was computed.

3D cell morphology measurements

Cell sizes along longitudinal, radial and circumferential directions were computed in MorphoGraphX[21] by first performing a Principal Component Analysis (PCA) on the voxels of segmented cells. Then the component of the PCA's tensor along the axis of interest was computed.

Shortest division plane estimation and comparison to actual division plane

To compute the relative division plane area, we used the following pipeline in MorphoGraphX which was adapted from Barbier de Reuille et al.[21] First, we calculated the center of actual division plane by calculating the center of gravity of the triangulated surface meshes of the shared wall between two neighboring daughter cells. Then the daughter cells of recently divided cells in segmented meshes were merged. The actual division plane was approximated as a flat wall by computing the principal components of the vertices that were located at the shared border of the two daughter cells. After we simulated a division using this flat wall to determine the surface area of the real division wall (A_real). Then the mean areas of the top 0.1% shortest (A_min) and longest division planes (A_max) in merged cells were determined by sampling of > 10000 division directions uniformly spread on the cell volume, going through the center of the actual division wall. Finally, we computed $\hat{A} = (A\_real - A\_min) / (A\_max - A\_min)$, where $\hat{A}$ is the relative cell wall area, A_min the area of the shortest sampled division planes, A_max the largest sampled division planes, and A_real the area of the flat approximation of the real cell wall.

Embryo isolation and transcriptome analysis

Ovules were collected from ~60 siliques using vacuum extraction. Siliques were stuck to double-sided tape and sliced open using a needle. Open siliques were submerged in 1x PhosphateBuffered Saline (PBS) buffer and ovules were collected using a vacuum pump through 50 μm filters. Collected ovules were then transferred to Isolation buffer (1x First Strand Buffer (FSB; Invitrogen), 1mM Dithiotreitol (DTT), 4% RNaseLater, MQ), and volume was reduced to ~20 μL. Embryo isolation was performed according to Raissig et al.[56] with the following adaptations. A Zeiss Confocor 1 inverted microscope (Carl Zeiss Microscopy GmbH, Jena, Germany) together with an Eppendorf Transferman 4r micromanipulator (Eppendorf AG) and VacuTip II microcapillaries (Eppendorf) were used to isolate about 40-50 washed embryos in 50 μL isolation buffer.

RNA was amplified using the Ovation Pico WTA System V2 (NuGEN, CA, USA), labeled with the ENCORE Biotin Module (NuGEN) and hybridized to *Arabidopsis* Gene 1.1 ST arrays (Affymetrix, CA, USA) according to the manufacturers protocol. Microarray analysis was performed using the MADMAX pipeline[57] and a custom CDF file (MBNI CustomCDF version 19.0.0).[58] Here, all expression values were (quantile) normalized by the Robust multi-array average algorithm (RMA).[59] Probe sets were redefined using current genome information[58] and re-organized according to TAIR10 gene definitions. Linear models and an intensity-based moderated t statistic

approach[60,61] were used to identify differentially expressed genes (probe sets). P values were corrected for multiple testing using an optimized false discovery rate (FDR) approach.[62]

QUANTIFICATION AND STATISTICAL ANALYSIS

Microsoft Excel was used to analyze the data. Plots-of-Data web app was used to plot measured data points, which is based on R.[63] All error bars are represented as median ± 95% confidence intervals for each sample and were calculated by percentile bootstrap method provided by the Plots-of-Data web app. Sample sizes for each experiment are depicted in figure legend.